Appl. Phys. B 50, 479–485 (1990)

Applied Physics B Photophysics and Laser Chemistry

Degenerate Four-Wave Mixing Diagnostics on OH and NH Radicals in Flames*

Thomas Dreier and David J. Rakestraw

Combustion Research Facility, Sandia National Laboratories, Livermore, CA 94551, USA

Received 14 November 1989/Accepted 8 February 1990

Abstract. Degenerate four wave mixing (DFWM) is applied as a diagnostic to study OH and NH radicals in flames. DFWM is a coherent technique which offers the advantages of a highly collimated signal beam permitting efficient rejection of interfering radiation and requiring minimal optical access. Rotational temperatures have been determined from the DFWM spectra and are in close agreement with the temperatures measured using coherent anti-Stokes Raman scattering of nitrogen.

PACS: 42.65 Hw, 82.40 Py, 42.65 Dr, 42.65 Ft

With the availability of high power tunable laser sources, optical spectroscopy has gained widespread application as a diagnostic to detect stable and reactive species in gas phase systems. Laser-based methods are nonintrusive and provide high spatial and temporal resolution when light pulses of nano- and picosecond duration are employed and probe volumes are reduced by overlapping or focussing the beams. These characteristics are especially attractive for combustion diagnostics applications.

Linear optical spectroscopies such as laser-induced fluorescence (LIF) [1, 2], absorption [3], Rayleigh [4], and spontaneous Raman scattering [5, 6] have found widespread application in mapping concentration profiles in flames. Spontaneous Raman- and Rayleigh scattering are mainly used for measuring temperatures, major species (N_2, O_2, H_2O, CO_2, fuel) concentrations and density due to their lower sensitivity. Laser-induced fluorescence and absorption techniques are generally employed for detecting trace reactive species (OH, CH, CN, NH_2, NH).

Nonlinear optical diagnostics have also proved very valuable. Among them, coherent anti-Stokes Raman spectroscopy (CARS) offers the capability to measure temperature and major species concentrations [8] even in hostile environments [9]. The coherent generation of the signal beam in this four-wave mixing process makes it ideal for remote probing and detection of otherwise difficult to access devices such as internal combustion engines [10]. To increase the detection sensitivity of the method the wavelengths of the participating wave mixing beams and the generated anti-Stokes beam can be tuned in the vicinity of electronic absorption transitions. This greatly increases the signal strength by resonance enhancement. Resonance CARS has been successfully demonstrated for iodine vapor [11] and recently for OH in premixed H_2/air and CH_4/air flames [12]. However, the high sensitivity of resonance CARS comes at the expense of increasing the experimental complexity and the complexity of spectral interpretation.

Another closely related nonlinear optical process involving the third order susceptibility $\chi^3(\omega)$ is degenerate four-wave mixing (DFWM). DFWM is widely used in measuring ultrafast relaxation and diffusion phenomena in liquids [13] and solids [14], and in optical phase conjugation [15]. It also has potential application in high resolution spectroscopy because of the Doppler free nature of the interaction process. Using only one laser wavelength the technique has

* Work performed at the Combustion Research Facility, Sandia National Laboratories, supported by the U.S. Department of Energy, Energy Conversion and Utilization Technologies Program and Office of Basic Energy Sciences, Division of Chemical Sciences

been demonstrated to be a sensitive detection method for sodium in flames [16, 17]. For molecules, lower sensitivity is expected because of the smaller transition moments involved. Nonetheless, Ewart and O'Leary [18] have succeeded in detecting OH radicals in a flame and demonstrated promising signal to noise ratios via several R_1-lines in the $A-X(0,0)$ ultraviolet absorption band.

In this paper, we present an extended investigation of DFWM spectroscopy of OH and NH radicals in atmospheric flames. By analyzing the individual rotational lines of the $A(^2\Sigma^+)-X(^2\Pi)$ (OH) and $A(^3\Pi)-X(^3\Sigma^-)$ (NH) transitions, temperatures in the overlap volume of the beams are determined. An independent comparison of these results was made by performing a nitrogen CARS temperature measurement at the same location in the flame under identical operating conditions of the burner.

1. Overview of DFWM

We use a DFWM geometry in which two pump waves $\mathbf{E}_f$ and $\mathbf{E}_b$ are counterpropagating and cross a third wave $\mathbf{E}_p$ at an angle Θ between $\mathbf{E}_p$ and $\mathbf{E}_f$, and where all waves are of identical frequency, ω. The nonlinear interaction couples these three waves to a fourth wave $\mathbf{E}_s(\omega)$ which counterpropagates with $\mathbf{E}_p$ and can be spatially separated through the use of a beamsplitter. This geometry meets the phase matching requirements for all angles Θ and has the unique property that $\mathbf{E}_s$ is proportional to the complex conjugate of $\mathbf{E}_p$, namely $\mathbf{E}_p^*$. The generated nonlinear polarization can be written [19, 20]

$$\mathbf{P}_s^{(3)}(\mathbf{k}_s=-\mathbf{k}_p,\omega)=A(\mathbf{E}_f\cdot\mathbf{E}_p^*)\mathbf{E}_b + B(\mathbf{E}_b\cdot\mathbf{E}_p^*)\mathbf{E}_f+C(\mathbf{E}_f\cdot\mathbf{E}_b)\mathbf{E}_p^*, \quad (1)$$

where A, B, and C are related to different tensor components of the third order susceptibility $\chi^{(3)}$, and also depend on Θ. A resonance enhancement of the DFWM signal occurs whenever ω matches an allowed molecular transition. Each of these three terms can be given a physical interpretation. The first two terms describe an interference of the $\mathbf{E}_p$ with $\mathbf{E}_f$ and $\mathbf{E}_b$. This interference gives rise to an optical fringe pattern in the sample such that the intensity of the light varies sinusoidally in the beam overlap region. In an absorbing medium, this spatial oscillation in intensity results in a corresponding variation in the concentration of excited states. These alternating regions have different indices of refraction and therefore form a Bragg grating. This volume diffraction grating produced by the interference of $\mathbf{E}_p$ and $\mathbf{E}_f$ ($\mathbf{E}_p$ and $\mathbf{E}_b$) then results in the scattering of $\mathbf{E}_b$ ($\mathbf{E}_f$). The third term in (1), which describes the interaction of $\mathbf{E}_f$ and $\mathbf{E}_b$, oscillates at 2ω and is not important for one-photon absorption processes. It becomes important for non-absorbing media and processes involving a near resonant two-photon absorption [20].

In the current experiment we use a configuration in which $\mathbf{E}_f$ and $\mathbf{E}_p$ have parallel polarizations that are oriented at 90° with respect to $\mathbf{E}_b$. Therefore, the first term in (1) is responsible for the generated wave $\mathbf{E}_s$ which will be polarized parallel to $\mathbf{E}_b$ [12, 21]. (No intensity interference pattern will be generated between the crossed polarized waves $\mathbf{E}_b$ and $\mathbf{E}_p$.) This geometry has been chosen for two reasons. First, it leads to scattering from the grating with the largest fringe spacing Λ ($\Lambda=\lambda_p/2\sin(\Theta/2)$), where $\Theta=4°$ for the first term compared to 176° for the second term of (1) [14]. This reduces effects of grating washout due to molecular motion which is significant for the high temperatures of flames. Second, the fact that $\mathbf{E}_p$ and $\mathbf{E}_s$ have polarizations that differ by 90° allows for efficient discrimination in the detection of $\mathbf{E}_s$ using a polarizer.

The description of the four-wave mixing interaction given above has ignored the contribution of orientational gratings that can result from vectorial addition of electric fields with crossed polarization [22]. In this case the electric field polarization varies from linear to left circular to linear to right circular and finally back to linear across one fringe. This results in a spatial variation in the M_J distribution of the excited molecules and can also result in diffraction. The importance of orientational gratings is generally smaller than that of population gratings but will strongly depend on the molecule of interest and the geometry and polarization of $\mathbf{E}_f$, $\mathbf{E}_b$, and $\mathbf{E}_p$.

A detailed theoretical description of the non-linear polarization generated by the four-wave mixing process was given by Abrams and Lind over one decade ago [23]. Investigations of more complicated systems have followed and included treatment of Doppler broadening, saturation phenomena, collisional effects, multiple level schemes, and effects of broadband lasers. A full treatment of our present experimental conditions which include all effects mentioned has not yet been attempted.

2. Experimental

Figure 1 shows the experimental setup used in this investigation. Tunable laser radiation (OH: 307 nm, NH: 335 nm range) is generated by frequency doubling the output of a tunable dye laser (Lumonics Hyperdye 300) pumped by the second harmonic output of a Nd:YAG laser (Quanta Ray DCR 2A). The frequency doubling unit Lumonics Hypertrack 1000) was tuned by a keypad-operated computer interface synchronously with a stepping of the dye laser grating to keep the doubling efficiency at its maximum. The

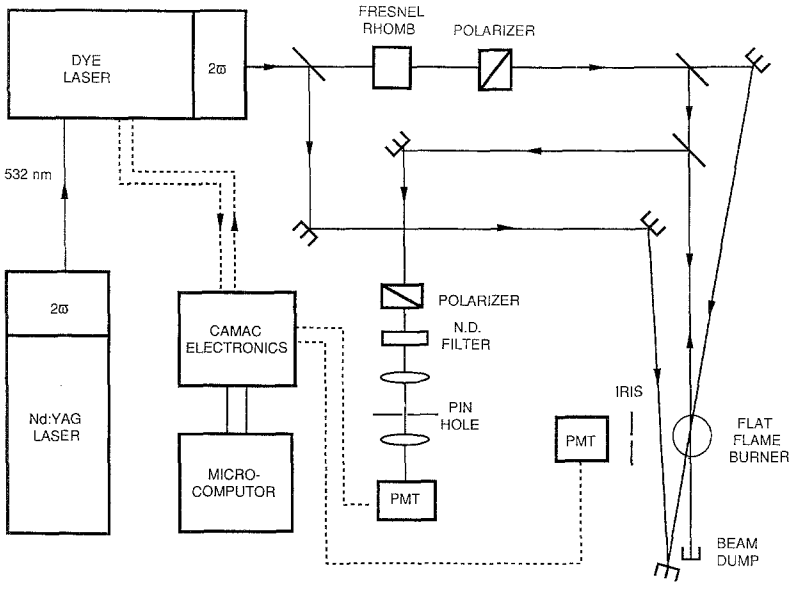

Fig. 1. Schematic diagram of the experimental setup for DFWM detection of radicals in a flame. PMT: photomultiplier tube. Laser induced fluorescence is collected at right angle to the intersecting laser beams in the flame

ultraviolet output radiation is split by a 30% reflectivity beamsplitter into collinear, counterpropagating forward and backward pump beams. A second beamsplitter and a quartz prism direct a low intensity probe beam under a crossing angle of 4.2° into the overlap region of the two pump beams. A beam diameter of 1.5 mm defines an overlap length of approximately 25 mm. To increase the spatial resolution of the sampling volume, in the case of the NH measurements, the backward pump beam was collimated to a diameter of approximately 0.5 mm. With a double Fresnel rhomb, a polarizer in the pump beam path and two polarizers in the probe beam path the intensities of both incoming beams can be varied independently and the pump beam polarizations can be rotated relative to that of the probe beam. The phase conjugated DFWM signal is split off with a 30% beamsplitter and directed to a photomultiplier (RCA 1P28A). To reduce stray and background light from reaching the detector the DFWM beam travels approximately 3 m through several apertures, a polarizer and is focussed through a 100 μm diameter pinhole.

In the case of OH, a LIF signal is observed simultaneously with the DFWM signal at right angle to the crossing beams in the burner by a second multiplier. An adjustable iris in front of this PMT (500 V) defines the viewing angle of light striking the photocathode but no special precautions have been taken to exactly match the DFWM and LIF probe volumes in the flame. A photodiode monitors the laser intensity of the probe beam. The energies of the individual beams are measured with a fast thermopile detector (Molectron J3-05). The electrical signals are preprocessed using standard CAMAC electronics and the data are stored in a laboratory computer (DEC Microvax II). The computer also controls the scanning of the dye laser by tuning slowly across the relevant lines while scanning fast in between lines.

CARS spectra are taken using part of the second harmonic output of the Nd:YAG laser to pump a broadband dye laser centered at the Stokes-shifted wavelength for nitrogen. The remaining part of the green light together with the dye laser output is overlapped and focussed with a 300 mm focal length lens into the flame gases forming a three-dimensional geometry [8]. Nonresonant reference spectra for normalizing the flame CARS spectra are acquired in a stainless steel cell filled with 3000 Torr of oxygen or propane. The CARS signal beam is dispersed in a 0.85 m double monochromator (SPEX Model 1402) and detected with a CCD camera (Photometrics 200 series). Normalized flame and room temperature spectra are transferred to a mainframe computer (VAX 8650) for temperature analysis. The CARS apparatus has been described in more detail elsewhere [25].

For OH detection stoichiometric premixed propane/air flames were run at a fuel flow rate of 5 l/min and a co-flow of nitrogen on a flat flame burner, which stabilizes the flame on a sintered stainless steel plate 50 mm in diameter. The burner housing was water cooled and the fuel flow was regulated with a Tylan flow controller. The DFWM and CARS measurement point was located 9 mm above the center of the burner surface. NH radicals were detected in an ammonia (2.1 l/min)/oxygen (1.5 l/min)/nitrogen (1.0 l/min) flame 1.6 mm above the burner surface. This close distance of the probing laser beams to the burner surface generated a considerable amount of stray light and therefore prevented the observation of LIF signals.

3. Results and Discussion

An assigned DFWM spectrum of the OH $A(^2\Sigma^+) - X(^2\Pi)$ transition taken 9 mm above the burner surface is shown in Fig. 2a. The simultaneously recorded LIF spectrum is shown as a dashed line. In general the signal-to-noise was limited by the dynamic range of our photomultiplier tube. However, the strong power dependence of the interaction resulted in large shot-to-shot variations in the signal intensities (in the absence of saturation, $\mathbf{E}_s \propto \mathbf{E}_p^* \mathbf{E}_f \mathbf{E}_b$). Therefore, each spectral point in Fig. 2 was an average of 20 laser shots.

The DFWM intensities depend on the square of the third-order nonlinear susceptibility and therefore are proportional to the square of the population difference of the resonant transition. By comparing signals from two different spectroscopic transitions that probe the same OH fine structure state we also find that the integrated DFWM signals are dependent on the square of the rotational line strengths. Several OH rotational states were examined using the R_1 and the R_{21} transitions of the (0,0) vibrational band which have significantly different line strengths. Using the relationship

$$I_{sig} \propto [B_{ij} N_{OH}(v'', J'')]^2, \tag{2}$$

where $N_{OH}(v'', J'')$ is the OH rotational state number density and B_{ij} is the one-photon line strength of the probed molecular transition [26], rotational populations were determined. The populations determined from these two branches for the first five rotational states were found to be in excellent agreement (within 10%). Table 1 compares the ratios of the line strengths to the square root of the ratios of the signal intensities for these two transitions demonstrating the validity of (2).

Using this relationship temperatures were derived from the integrated intensities of well-resolved transitions in the R_1 and R_2 rotational branches. Using the assumed Boltzmann distribution within the rotational manifold

$$N_N(v=0) \propto (2J+1)\exp(-\Delta E_N hc/kT), \tag{3}$$

where ΔE_N is the term value of rotational level $J = N \pm 1/2$, and the squared dependence of the line intensities on population, a plot of

$$\ln\left(\frac{\sqrt{I_{sig}}}{[2(N \pm \frac{1}{2})+1]B_{ij}}\right) \tag{4}$$

versus rotational energy should give a straight line. A temperature is then derived from the slope of a linear least squares fit to the experimental data points. A typical Boltzmann plot determined from one spectral scan of OH is shown in Fig. 2b.

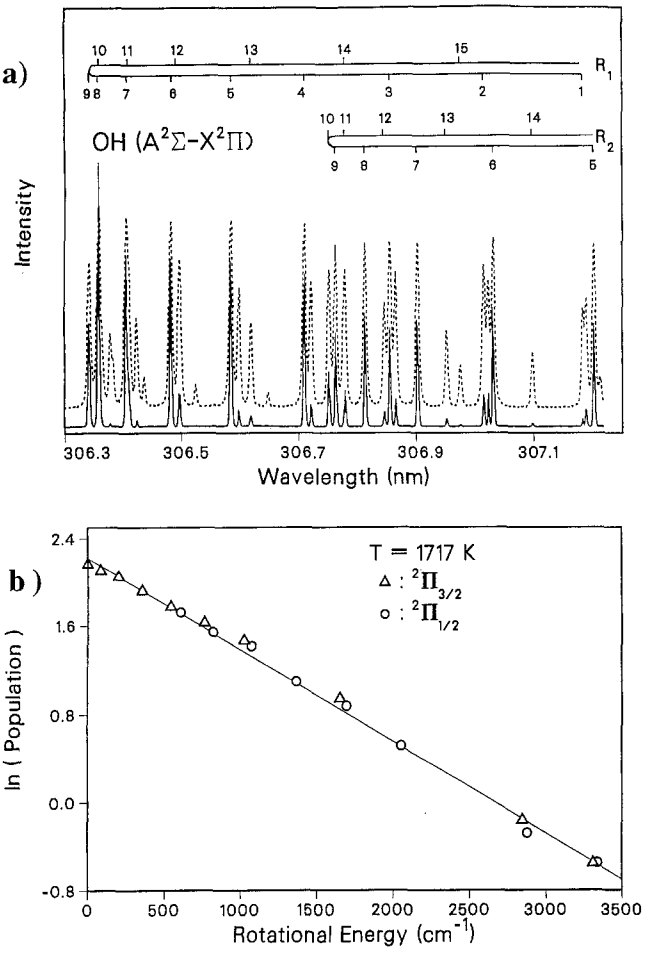

Fig. 2. **a** Simultaneous recording of the DFWM (solid line) and LIF (dashed line) signals for the OH $A(^2\Sigma^+) - X(^2\Pi)$ transition as a function of doubled dye laser wavelength. Pump beam energy: 780 μJ; probe beam energy: 74 μJ. For clarity the LIF spectrum is offset with respect to the DFWM spectrum baseline by an arbitrary amount. The vertical scale is in arbitrary intensity units. **b** Boltzmann plot of OH population distribution derived from DFWM spectrum as shown in **a**. In the analysis R_1 (triangles) and R_2 (circles) transitions are used. Solid line: least squares linear regression through the data points

Table 1. Comparison of measured ratios of main (I_{R_1}) and satellite ($I_{R_{21}}$) DFWM line intensities with calculated ratios of the corresponding line strengths (LS) after [26]. Pump beam energy: 844 μJ, probe beam energy: 32 μJ

N	$LS(R_1)/LS(R_{21})$	$[I_{R_1}(N)/I_{R_{21}}(N)]^{1/2}$
1	0.667	0.68
2	1.19	1.3
3	1.84	1.8
4	2.63	2.7
5	3.55	3.5

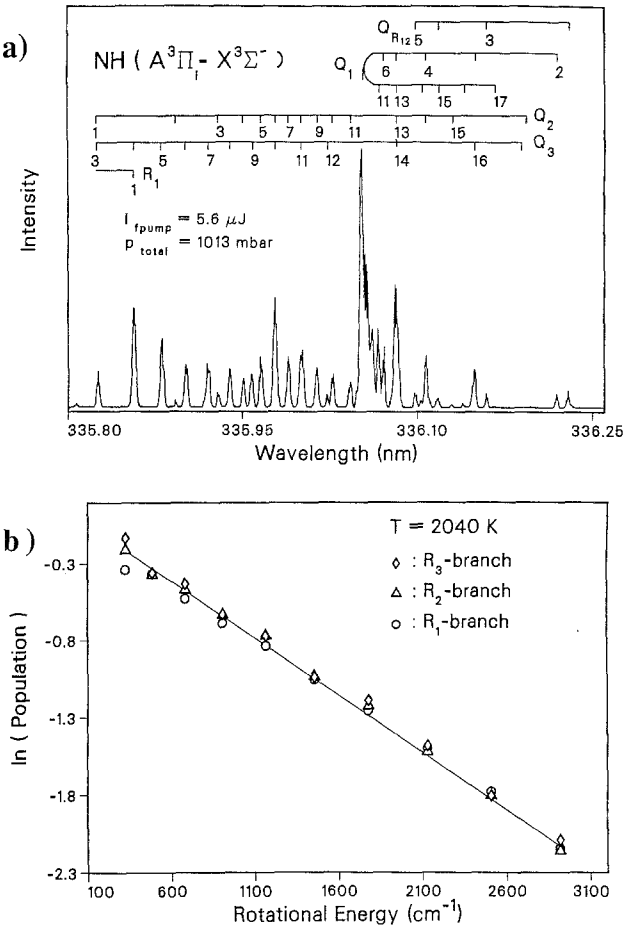

Fig. 3. **a** Experimental DFWM rotational spectrum of the Q-branch region of the NH ($A^3\Pi - X^3\Sigma^-$) transition taken in a 1 atm pressure $NH_3/O_2/N_2$ flat flame 1.6 mm above the burner surface. The transitions are labeled by the ground state total angular momentum quantum number N. **b** Boltzmann plot of rotational population distribution in the R-branches of the NH ($A^3\Pi - X^3\Sigma^-$) (0,0) electronic transition. The straight line is a regression line through all data points, giving a temperature of 2042 K

Analogous measurements have been made on the NH radical in an ammonia/oxygen/nitrogen flame close to the burner surface. A DFWM spectrum of NH in the Q-branch region of the $A(^3\Pi)$–$X(^3\Sigma^-)$ transition is shown in Fig. 3a. The DFWM signals obtained for NH in this flame were exceptionally strong and spectra with good signal-to-noise ratios could be obtained using a total laser intensity of 10 kW/(cm^2 wavenumber). Because of the spectral congestion in the Q-branch region, populations were determined from the neighboring three R-branches (330.9–335.6 nm). A Boltzmann plot resulting from such a scan is shown in Fig. 3b.

In order to test the accuracy of the temperatures determined using DFWM, CARS measurements were undertaken at the same spatial location in the flames to deduce temperatures from molecular nitrogen CARS Q-branch spectra. Theoretical CARS signatures are generated and fitted to averaged CARS spectra covering the $v = 0$–1, 1–2 Raman transitions with band heads at 2330 and 2303 cm^{-1}, respectively, in a least squares fit computer routine. The temperatures determined using DFWM and CARS are compared in Table 2. Excellent agreement is found for both OH and NH. The error limits for the CARS temperatures are deduced from the final fitting values of several data sets. The low concentration of the nitrogen seeded ammonia flame caused the CARS signal to decrease appreciably compared to the propane/air flame. The noticable nonresonant background interference in the generated CARS spectra also contributed to the increase in the error limits of the measurements. Temperature gradients were found to be negligible with respect to our spatial resolution in the postflame gases for the OH measurements. However, gradients near the flame front in the case of the NH measurements are certainly important and spatial averaging in the probe volume [27] limits the accuracy of the temperature measurements in both methods used. The agreement of measured temperatures using DFWM and CARS along with the data presented in Table 1 demonstrates the ability to easily interpret the DFWM signal intensities using the very simple relation given in (1).

Table 2. Flame conditions and temperature measurement results using CARS and DFWM diagnostics

Flame	Volume flows [l/min]	T_{CARS} [K]	T_{DFWM} [K]
C_3H_8/air	$\Phi(C_3H_8)$: 5 Φ(air): 48	1703±20	1730±60
$NH_3/O_2/N_2$	$\Phi(NH_3)$: 2.1 $\Phi(O_2)$: 1.5 $\Phi(N_2)$: 1.0	2100±150	2042±106

In the experiments described here to determine temperatures, the laser intensities used were in excess of the saturation intensity for the one-photon transitions. In the case of OH, I_{sat} is approximately 1 MW/(cm^2 wavenumber) [28] and laser intensities in the range of 5–12 MW/(cm^2 wavenumber) were used in the experiments. The effects of saturation on the one-photon transitions are most apparent from the examination of the LIF spectrum acquired simultaneously with the DFWM spectrum shown in Fig. 2. As can be seen in Fig. 2 the DFWM lines are narrower than the LIF linewidths due in part to the square dependence of the DFWM intensities on the susceptibility. The FWHM linewidths in the LIF spectrum are

measured to be $\sim 0.40\,cm^{-1}$. In addition to the broadening due to saturation, this linewidth is composed of a laser linewidth of $\sim 0.15\,cm^{-1}$, and a calculated Doppler and collision width of $\sim 0.25\,cm^{-1}$ and $\sim 0.07\,cm^{-1}$ [29], respectively. Both the DFWM and the LIF linewidths were observed to narrow as the laser intensity was lowered. The laser-induced absorption rate, W_{12}, for the OH[$R_1(7)$] transition [30] at pump energies of 500 μJ (~ 7 MW/(cm^2 wavenumber)) is $\sim 5 \times 10^{10}\,s^{-1}$ which is much larger than the decay rate of the excited level due to spontaneous emission and rotational relaxation of $\sim 1.5 \times 10^9\,s^{-1}$. Therefore, the stimulated pumping rate is dictating the lifetime of the electronically excited OH rather than collisional removal. This should reduce problems associated with rotational level dependent quenching which in some cases requires corrections to be made in the analysis of LIF spectra. It should also be noted that self-absorption was determined not to be a serious problem in the present experiments and consequently did not contribute significantly to the observed linewidths.

An additional note should be made concerning saturation effects on the rotational populations measured using the R_1 and the R_{21} transitions. As discussed earlier these two branches probe the same state but have considerably different rotational line strengths. The difference in line strengths for the R_1 and the R_{21} transitions results in a disagreement in the measured population when using LIF in the saturated regime (i.e. the population is no longer linearly proportional to the line strengths). However, the degree of saturation at the one-photon level does not seem to perturb the squared dependence of the DFWM intensities on the line strengths as shown in Table 1. We offer no explanation of this at the present time. Further experiments to understand the effects of saturation are in progress.

In this article we have demonstrated the usefulness of degenerate four-wave mixing (DFWM) for combustion diagnostics of transient species. The method was applied to the detection of the OH and NH radicals in premixed atmospheric pressure flat flames. Using the R-lines of the OH $A(^2\Sigma^+) - X(^2\Pi)$ and the NH $A(^3\Pi) - X(^3X^-)$ systems, temperatures were derived from Boltzmann plots. These temperatures lie within the error limits of CARS temperature measurements using nitrogen as the Raman active species. DFWM is very attractive for combustion applications due to the coherent nature of the generated signal beam which gives a high collection efficiency and makes stray light rejection and remote probing easy in hostile and luminous environments. Other advantageous features include the polarized signal radiation and high spatial and temporal resolution. In addition DFWM reveals the high sensitivity of a resonance enhanced CARS process without being experimentally too complicated. Finally the high sensitivity and low laser intensity requirements make two-dimensional imaging feasible. This was first demonstrated for atomic sodium [31] and has recently been applied to OH in this laboratory.

Acknowledgements. The authors would like to thank G. O. Sitz for providing them the line integration and fitting program, R. E. Palmer for support of the Sandia CARS code, J. B. Jeffries for providing us with NH line strengths, and L. A. Rahn, F. P. Trebino, and R. L. Farrow for helpful discussions. TD is thankful to the Deutsche Forschungsgemeinschaft for the grant No. Dr 195/1-1. Work performed at the Combustion Research Facility, Sandia National Laboratories, and supported by the U.S. Dept. of Energy, Energy Conversion and Utilization Technologies Program and Office of Basic Energy Sciences, Division of Chemical Sciences.

References

1. J.H. Bechtel, R.E. Teets: Appl. Opt. **18**, 4138 (1979)
2. R.P. Lucht, D.W. Sweeney, N.M. Laurendeau: Comb. Sci. Technol. **42**, 259 (1985)
3. M.S. Chou, A.M. Dean, D. Stern: J. Chem. Phys. **76**, 5334 (1982)
4. R.W. Dibble, R.W. Hollenbach: 18th Int'l Symp. on Combustion (The Combustion Institute, Pittsburgh 1981) p. 1489
5. R.W. Dibble, A.R. Masri, R.W. Bilger: Comb. Flame **67**, 189 (1987)
6. M.C. Drake: Spontaneous Raman Scattering for Gas Phase Diagnostics, General Motors Report 6267, July 1988
7. R.K. Hanson: 21st Int'l Symp. on Combustion (The Combustion Institute, Pittsburgh 1986) p. 1677
8. A.C. Eckbreth: *Laser Diagnostics for Combustion Temperature and Species* (Abacus Press, Cambridge, Mass. 1988)
9. A.C. Eckbreth, G.M. Dobbs, J.H. Stufflebeam, P.A. Tellex: Appl. Opt. **23**, 1328 (1984)
10. R.P. Lucht, D. Dunn-Rankin: CARS Measurements of Thermal Boundary Layer Development in an Internal Combustion Engine, Paper presented at the spring meeting of the Western States Section/The Combustion Institute, Provo, Utah, March 1988
11. B. Attal, O.O. Schnepp, J.-P. Taran: Opt. Commun. **24**, 77 (1978)
12. B. Attal-Tretout, P. Bouchardy: La Rech. Aerosp. **5**, 19 (1987)
13. T.S. Rose, W.L. Wilson, G. Wackerle, M.D. Fayer: J. Chem. Phys. **86**, 5370 (1987)
14. H.J. Eichler, D. Pohl, P. Gunter: In *Laser Induced Dynamic Gratings*. Springer Ser. Opt. Sci., Vol. 50 (Springer, Berlin, Heidelberg 1986)
15. D.M. Pepper: IEEE J. QE-**25**, 312 (1989)
16. J. Pender, L. Hesselink: Opt. Lett. **10**, 264 (1985)
17. J.M. Ramsey, W.B. Whitten: Anal. Chem. **59**, 167 (1987)
18. P. Ewart, S.V. O'Leary: Opt. Lett. **11**, 279 (1986)
19. For a detailed description of the DFWM process and its applications see: *Optical Phase Conjugation*, ed. by R.A. Fisher (Academic, New York 1983)
20. J.F. Reintjes: In *Nonlinear Optical Parametric Processes in Liquids and Gases* (Academic, Orlando 1984)
21. D.G. Steel, R.C. Lind, J.F. Lam, C.R. Giuliano: Appl. Phys. Lett. **35**, 376 (1979)

22. R. Trebino, C.E. Barker, A.E. Siegman: IEEE J. QE-**22**, 1413 (1986)
23. R.L. Abrams, R.C. Lind: Opt. Lett. **2**, 94 (1978)
24. R.L. Farrow, P.L. Mattern, L.A. Rahn: In *Proceedings of the VII. International Conference on Raman Spectroscopy*, ed. W.F. Murphy (North-Holland, New York 1980) p. 668
25. R.P. Lucht, R.E. Teets, R.M. Green, R.E. Palmer, C.R. Ferguson: Combust. Sci. Technol. **55**, 41 (1987)
26. I.L. Chidsey, D.R. Crosley: J. Quant. Spectr. Radiat. Transf. **23**, 187 (1980)
27. J.P. Boquillon, M. Pealat, M. Bouchardy, P. Collin, P. Magre, J.P. Taran: Opt. Lett. **13**, 722 (1988)
28. J.T. Salmon, N.M. Laurendeau: Appl. Opt. **24**, 1313 (1985)
29. E.C. Rea, A.Y. Chang, R.K. Hanson: J. Quant. Spectr. Radiat. Transf. **37**, 117 (1987)
30. R.P. Lucht: In *Laser Spectroscopy and Its Applications*, ed. by L.J. Radziemski, R.W. Solarz, J.A. Paisner (Dekker, New York 1987)
31. P. Ewart, P. Snowdon, I. Magnusson: Opt. Lett. **14**, 563 (1989)